

Title: Interaction between Dry Granular Flow and Rigid Barrier with Basal Clearance: Analytical and Physical Modelling

Authors: Choi, C.E., Ng, C.W.W., Liu, H.*, and Wang, Y.

First-author

Name: Dr Clarence Edward Choi

Affiliation: Department of Civil and Environmental Engineering, The Hong Kong University of Science and Technology; The HKUST Jockey Club Institute for Advanced Study, HKSAR; HKUST Fok Ying Tung Graduate School, Guangzhou, China

Address: The Hong Kong University of Science and Technology, Clear Water Bay, Kowloon, Hong Kong

Email: ceclarenc@ust.hk

Co-author

Name: Dr Charles Wang Wai Ng

Affiliation: Department of Civil and Environmental Engineering, The Hong Kong University of Science and Technology

Address: The Hong Kong University of Science and Technology, Clear Water Bay, Kowloon, Hong Kong

Email: cecwwng@ust.hk

Corresponding author*

Name: Mr Haiming Liu

Affiliation: Department of Civil and Environmental Engineering, The Hong Kong University of Science and Technology

Address: The Hong Kong University of Science and Technology, Clear Water Bay, Kowloon, Hong Kong

Email: hliubc@ust.hk

Tel: +852 54498463

Co-author

Name: Dr Yu Wang

Affiliation: Department of Architecture and Civil Engineering, City University of Hong Kong

Address: City University of Hong Kong, Tat Chee Avenue, Kowloon, Hong Kong

Email: yuwang@cityu.edu.hk

Interaction between Dry Granular Flow and Rigid Barrier with Basal Clearance: Analytical and Physical Modelling

Choi, C.E., Ng, C.W.W., Liu, H.* , and Wang, Y.

ABSTRACT: Some types of barriers are designed with a clearance between the bottom of the barrier and the channel bed. This feature allows small discharges to pass, thereby reducing the maintenance required over the service life of the barrier. Aside from the practical function of a clearance, it influences the impact force, the jump height and discharge. In this paper, a series of physical experiments were conducted using a 6-m-long flume to model the interaction between dry granular flow and rigid barrier with a basal clearance. The ratio between the clearance and particle diameter H_c/D was varied from 0 to 10. The channel inclination was varied from 15° to 35° to achieve different Froude numbers before impact. A new impact model for predicting the impact force exerted on the barrier with a basal clearance is presented and evaluated. Results reveal that $H_c \geq 3D$ is capable for reducing the impact force and overflow. Findings from this study highlight the importance of considering the effects of basal clearance on the design of multiple-barrier systems.

Keywords: basal clearance; dry granular flow; rigid barrier; flume modelling

Introduction

Structural countermeasures such as rigid and flexible barriers are commonly constructed to mitigate the steep creek hazards (Kwan 2012; Sun and Law 2015; Moase et al. 2017). To minimise maintenance for barriers, a clearance (Fig. 1) is often prescribed between the base of the barrier and the channel bed (Volkwein 2014; Wieser 2014; Gems et al. 2014; Piton and Recking 2015; Chiari et al. 2016; Nagl et al. 2016a, 2016b). Sze and Lam (2017) reported a summary of overseas guidelines on the design of flexible barriers spanning the entire width of the stream courses. Findings recommended that barriers need a suitably-sized basal clearance to prevent the accumulation of stream loads so as to reduce the maintenance required. Some proprietary products were reported to allow basal clearances that range from 0.5 m to 1.5 m (Sze and Lam 2017). However, the recommendations remain based on an empirical criterion.

Wendeler and Volkwein (2015) carried out a series of laboratory tests to study the influence of both the mesh size opening and basal clearance on the retention volume of a net barrier. Findings revealed that the net barrier achieved an optimal retention volume by sizing both the mesh size opening and basal clearance based on d_{90} , representing particle size larger than 90% of the debris material. Their study laid a strong foundation for designing net barriers based on volume retention. However,

the effects of a basal clearance on the impact load and jump height remain a topic of practical and scientific interest in the mitigation of steep creek hazards.

Discharge through a basal clearance is expected to affect the deposited material at the base of the barrier, referred to as dead zone herein (Faug et al. 2002; Gray et al. 2003). The dead zone plays an important role in exerting static load (Caccamo et al. 2011) and altering the flow kinematics and the resulting force on the barrier as debris rides overtop the dead zone (Faug et al. 2012).

Understanding the effects of a basal clearance is particularly important when designing multiple-barrier systems (WSL 2008; Wendeler et al. 2008; Kwan et al. 2015) in steep creeks. A basal clearance can directly influence the volume of material retained and the volume of material allowed to discharge downstream. The material that discharges downstream can pass through the basal clearance or overflow the barrier (Hákonardóttir et al. 2003a, 2003b; Naaim-Bouvet et al. 2004; Choi et al. 2014; Speerli et al. 2010; Glassey 2013; Kwan et al. 2015; Ng et al. 2018) once the retention capacity of the barrier is reached. More importantly, overflow has been recognised as a key mechanism that is responsible for scouring of the channel bed that is just downstream of the barrier (Comiti et al. 2013; Chen et al. 2016). This process compromises the geotechnical stability of barrier foundations (Hübl et al. 2005). With these considerations in mind, it is evident that a basal clearance plays a critical role in

flow-barrier interaction and warrants further attention in the design of barriers.

In this study, a series of small-scale physical experiments were carried out to study the interaction between dry granular flow and rigid barrier with a basal clearance. The influences of the size of the basal clearance on discharge, jump height and impact force were investigated. Furthermore, a new impact model for barriers with a basal clearance is presented and evaluated.

Momentum jump model to predict jump height

Prediction of jump height is important in determining the design height of a barrier (Iverson et al. 2016; Ng et al. 2018). An analytical solution originating from Hákonardóttir et al. (2003b) for calculating the jump height directly behind a closed barrier has been applied to snow avalanches (Jóhannesson et al. 2009), debris flow (Iverson et al. 2016) and granular flows (Faug 2015a; Albaba et al. 2018). The analytical solution considers continuous and uniform flow impacting a closed stationary barrier. The impact process causes the frontal velocity to decelerate completely and jump upwards (Choi et al. 2015; Iverson et al. 2016). A modified form, which accounts for different lateral earth pressure coefficients, was reported by Iverson et al. (2016) and is given as follows:

$$(1) \quad \left(\frac{\rho_j}{\rho_i}\right)^2 \left(\frac{h_j}{h_i}\right)^3 - \frac{\rho_j}{\rho_i} \left(\frac{h_j}{h_i}\right)^2 - \left(\frac{2}{k} Fr_i^2 + 1\right) \frac{\rho_j h_j}{\rho_i h_i} + 1 = 0$$

where ρ is the bulk flow density; h is the flow depth; subscripts “i” and “j” (Fig. 2)

indicate flow properties of the initial upstream flow and the jump at the barrier, respectively. Variable h_j is therefore the jump height of the flow after impact. k is the lateral earth pressure coefficient, denoting the ratio of longitudinal to normal stresses, and may vary over a broad range. Iverson et al. (2016) reported values of k from 0.2 to 5 for frictional flows. Fr is the Froude number, which is the ratio of the inertial to gravitational forces in an open channel flow and given as follows:

$$(2) \quad Fr_i = \frac{v_i}{\sqrt{gh_i \cos \theta}}$$

where v is the flow velocity, g is the gravitational acceleration ($g = 9.81 \text{ m/s}^2$ in this study), and θ is the channel inclination.

Faug (2015a) and Albaba et al. (2018) further solved eq. (1) with Cardano's method (Cardano and Spon 1968), assuming $k = 1$, for the jump height h_j , which is given as follows:

$$(3) \quad \xi = \frac{h_j}{h_i} = 2r^{1/3} \cos\left(\frac{\theta_0}{3}\right) + \frac{1}{3\lambda_\phi}$$

where ξ is the jump height ratio, λ_ϕ is the density ratio and can be expressed as $\lambda_\phi = \rho_j/\rho_i$. r and θ_0 are expressed as following:

$$(4) \quad r = \frac{1}{2}\sqrt{q^2 - \Delta}$$

$$(5) \quad \theta_0 = \arccos\left(-\frac{q}{2r}\right)$$

where $\Delta = q^2 + 4p^3/27$, q and p are functions of Fr_i and λ_ϕ :

$$(6) \quad q = \frac{1}{\lambda_\phi^2} \left(1 - \frac{1 + 2Fr_i^2}{3} - \frac{2}{27\lambda_\phi} \right)$$

$$(7) \quad p = -\frac{1 + 2Fr_i^2}{\lambda_\phi} - \frac{1}{3\lambda_\phi^2}$$

Assuming that the density of the flow remains unchanged, λ_ϕ is unity in eq. (3).

ξ , r and θ_0 can be rewritten as follows:

$$(8) \quad \xi = 2r^{1/3} \cos\left(\frac{\theta_0}{3}\right) + \frac{1}{3}$$

$$(9) \quad r = \sqrt{\frac{1}{27} \left(2Fr_i^2 + \frac{4}{3} \right)^3}$$

$$(10) \quad \theta_0 = \arccos \left[\frac{\left(Fr_i^2 - \frac{8}{9} \right)}{\sqrt{3 \left(2Fr_i^2 + \frac{4}{3} \right)^3}} \right]$$

Although assuming a constant density simplifies the impact process by treating the flow as incompressible, it provides a more conservative prediction of larger jump height as reported by Faug et al. (2015). The jump height ratio ξ can thus be solved using only one unknown parameter, which is the Froude number of the incoming flow.

Newly-proposed impact model for barriers with basal clearance

A simplified approach based on the conservations of mass and momentum (Hübl et al. 2009; Scheidl et al. 2012, 2013; Ng et al. 2017b) is commonly recommended in design guidelines (VanDine 1996; MLR 2006; NILIM 2007; Kwan 2012) to predict the impact force on barriers. This hydrodynamic approach explicitly considers dynamic loading and the equation is given as follows:

$$(11) \quad F_{dy} = \alpha \rho_i v_i^2 h_i w$$

where α is dynamic pressure coefficient and w is the channel width. Recently, Wendeler et al. (2018) reported a load model that combines both the hydrostatic and hydrodynamic components for a steel net barrier with basal clearance. The hydrodynamic model in eq. (11) and the model proposed by Wendeler et al. (2018) are ideal for design because only a small number of parameters, which can be obtained with ease, are required. However, both the two load models do not consider the effects of barrier opening and may lead to an overestimation of the impact force.

In this study, a new impact model considering the basal clearance in a rigid barrier is proposed. Figure 2 shows that when granular flow impacts a rigid barrier with a basal clearance, a jump forms just upstream of the barrier and a steady discharge passes downstream through the basal clearance. Variable Q represents the flow rate and subscript “d” indicates discharge properties. Variable v_n is the propagation velocity of the granular jump. In this study, h_j is estimated using eq. (3) for simplicity. Equation (3) proposed by Albaba et al. (2018) strictly holds for flow impact against a rigid and closed barrier, without any discharge downstream of the barrier. However, we consider here that eq. (3) can be used as a first approximation for the estimation of the jump height in presence of the downstream discharge. Details on how basal clearance influences jump height will be discussed later.

The proposed impact model for a barrier with a basal clearance assumes a steady state control volume from the granular jump to the discharge (Fig. 2). All boundaries are assumed to be frictionless. The conservations of mass and momentum within a control volume are expressed as follows:

$$(12) \quad \rho_j h_j v_j - \rho_d h_d v_d = 0$$

$$(13) \quad w \int_0^{h_j} \sigma_{xj} dy - w \int_0^{h_d} \sigma_{xd} dy - F = \rho_j h_j w v_j (v_d - v_j)$$

where F is the impact force from the flow, σ_{xj} and σ_{xd} are the longitudinal normal stresses of the flow and can be simplified as $\sigma_{xj} = k\rho_j g(h_j - y)\cos\theta$ and $\sigma_{xd} = k\rho_d g(h_d - y)\cos\theta$. The internal energy dissipation during the discharge is ignored to provide a first-order approximation of the impact force. Therefore, assumption for solving eqs. (12) and (13) requires the energy at flow surfaces of the granular jump and discharge remains constant. This condition can be further expressed by Bernoulli's equation as follows:

$$(14) \quad \frac{\rho_j v_j^2}{2g\cos\theta} + \rho_j h_j = \frac{\rho_d v_d^2}{2g\cos\theta} + \rho_d h_d$$

In this study, the density of the discharge flow is also assumed unchanged to achieve a first-order approximation of the impact force, i.e., $\rho_i = \rho_j = \rho_d$. Moreover, we assume that the surface of the open-channel flow is only subjected to atmospheric pressure, and thus the pressure terms in eq. (14) are eliminated. The impact force F can therefore be expressed as follows:

$$(15) \quad F = \frac{\rho_i g (h_j - h_d)^3 w \cos \theta}{2(h_j + h_d)}$$

Substituting h_j with eq. (3), F can be rewritten as follows:

$$(16) \quad F = \frac{\rho_i g (h_i \xi - h_d)^3 w \cos \theta}{2(h_i \xi + h_d)}$$

The discharge flow depth h_d is governed by the basal clearance height and is assumed equal to the height of the basal clearance in this study. The impact force F can then be calculated using upstream flow parameters, which include the density, velocity, depth and width of the flow, and by knowing the basal clearance height and channel inclination. For a closed barrier with $h_d = 0$, eq. (16) can be written as follows:

$$(17) \quad F_s = \frac{\rho_i g h_i^2 \xi^2 w \cos \theta}{2}$$

which is, in essence, the hydrostatic force of the retained flow. A similar approach to eq. (17) for calculating the impact force on a closed rigid barrier has been proposed by Zanuttigh and Lamberti (2006) by adopting an approximate solution of the jump height ratio ξ based on the condition that an incoming Froude number is much larger than unity. Equation (11) can be written as a function of Froude number, Fr , as follows:

$$(18) \quad F_{dy} = \alpha Fr_i^2 \rho_i g h_i^2 w$$

If we divide eq. (18) by eq. (17), a relationship between the hydrodynamic equation and eq. (17) is given as follows:

$$(19) \quad \frac{F_{dy}}{F_s} = \frac{2\alpha Fr_i^2}{\xi^2 \cos \theta}$$

where ξ is a function of the Froude number, Fr_i , of incoming flow as expressed in

eqs. (8) to (10). When $Fr_i \gg 1$, it can be calculated from eqs. (8) to (10) that $2Fr_i^2/\xi^2 = 1$, and therefore $F_{dy}/F_s = \alpha/\cos \theta$.

Flume modelling

The experiments in this study were conducted using a 6-m-long flume model with a rectangular channel. The width and depth of the channel were 200 mm and 500 mm, respectively. At the upstream end of the flume, a container with a maximum volume of 0.1 m³ was used to store the granular material, which was retained by a gate. The gate was controlled using a magnetic lock at the base of the channel. Upon deactivation of the magnetic lock, the pneumatic gate was lifted vertically to release the granular material down the channel.

Flow characterisation

Characterisation of the flow before impact is important for correlating the dynamics of a flow and the resulting load. The Froude number, Fr , governs the dynamics of open-channel flow and is closely correlated with the impact behaviour on structures (Hübl et al. 2009; Armanini et al. 2011; Choi et al. 2015; Ng et al. 2017b).

For practical applications, knowledge of both the velocity and depth of the flow is convenient for characterising the dynamics of steady open-channel flows and correlating the dynamics with the impact behaviour. A diminishing Fr ($\ll 1$) indicates

that the effects of gravity and therefore static loading is significant. By contrast, $Fr \gg 1$ suggests that the existing state of inertia in the flow and therefore the dynamic loading is very much significant (Faug 2015b; Sovilla et al. 2016). In this study, different Fr were achieved by varying the channel inclination.

Instrumentation

Figure 3 shows a side schematic of the flume and the instrumentation used in this study. A high-speed camera (Fig. 3a; model no.: Mikrotron, EoSens® mini2) was installed at the side of the channel to capture the impact kinematics and to approximate both the flow depth and flow velocity for each test. Images were sampled at 300 frames per second at a resolution of 1660×970 pixels.

The rigid barrier (Fig. 3b) adopted in this study consisted of four 10-mm-thick acrylic plates. Each plate was instrumented with a load cell to measure the impact load along different locations of the barrier. The height of each acrylic plate near the bottom of the barrier was 50 mm and the acrylic plate near the top of the barrier had a height of 100 mm. A wooden plate was installed at the upper portion of the barrier and lined with plastic film to ensure a flush surface with the rest of the barrier. The instrumented barrier was 500 mm in height and mounted 1100 mm away from the gate of the storage container.

Test programme

Before conducting tests to study the interaction between dry granular flows and a rigid barrier with different basal clearances, control tests were carried out to characterise the Froude number of the flows without installing any barrier. The flow velocity and flow depth used to deduce the Froude number were measured based on high-speed camera images. The maximum flow depth at the barrier location was used to calculate the Froude number in eq. (2). Figure 4 shows a side schematic of the control test for determining the frontal velocity of the flow. The dilute flow front usually had a much higher velocity that was not representative of the flow. Correspondingly, the frontal velocity for each test was calculated using the thicker part of the flow front, which was ± 50 mm from the barrier location.

To discern the differences between fine and coarse granular flows, monodisperse glass spheres with diameters D of 3 mm and 10 mm were selected. The ratios between the flume width and the particle diameters, w/D , for the 3 mm and 10 mm spheres are 67 and 20, respectively. The initial bulk densities for the 3 mm and 10 mm glass spheres were 1620 and 1611 kg/m³, respectively. The measured dynamic friction angles for the 3 mm and 10 mm glass spheres were 17.8° and 16.6°, respectively (Ng et al. 2017a).

The channel inclination θ was varied from 15° to 35° to achieve different Fr . The

height of basal clearance was varied from 0 mm to 30 mm. The normalised basal clearance H_c/D , which is also regarded as the relative opening of the clearance, was ranged from 0 to 10 in this study. A summary of the test programme and measured Fr at the location of the rigid barrier is given in Table 1.

For each test a mass of 30 kg of glass spheres was prepared into the storage container with a horizontal free surface. Afterwards, the flume was inclined using a crane. When the channel inclination exceeded the repose angle of the granular material, the free surface of the granular material adjusted itself accordingly. This caused the initial heights, $H_{initial}$, of the source material to differ with different channel inclinations (Fig. 3a). Correspondingly, an increase in $H_{initial}$ could cause a slight increase of the flow depth near the container after initiation. This effect appeared to be more pronounced with the rather short transportation distance of 1100 mm that was modelled between the gate and the barrier.

Interpretation of test results

Observed kinematics of flow impacting barrier with basal clearance

Figure 5 shows a comparison between the observed kinematics captured using the high-speed camera and the velocity fields analysed using particle image velocimetry (White et al. 2003) for test C30-I35-D10. In this test, the channel was inclined at 35° , and the rigid barrier had a basal clearance with a relative opening $H_c/D = 3.0$.

The thin flow front passed through the basal clearance freely since the flow depth was smaller than the height of the basal clearance. As the tapered flow front became thicker, the flow started to interact with the barrier. From image analysis (Fig. 5a), the velocity vectors of the resisted flow near the base of the barrier changed direction from a predominantly slope parallel direction to a barrier parallel direction. At this stage of the impact process, the flux entering the system was larger than that passing underneath the barrier. The confining stress from the accretion of granular material just upstream of the barrier resisted the subsequent discharge of material underneath the barrier. Eventually, a distinct dead zone developed at the toe of the barrier (Fig. 5b). At this instant, a drastic reduction in discharge underneath the barrier occurred. Any additional discharge through the clearance was from the disintegration of the dead zone. Furthermore, the dead zone acted as a cushion against subsequent dynamic load exerted on the barrier. This is analogous to a series of force chains that redistribute stress in a granular assembly (Tordesillas et al. 2014). Figure 5c shows discharge was passing through the basal clearance without an upstream supply of granular material. Eventually, the discharge behaved like hopper flow (Ketterhagen et al. 2009), which was predominantly gravity-driven.

Jamming at the basal clearance

Jamming at the basal clearance was observed in the experiments with a relative

opening $H_c/D = 1.5$. Figure 6 shows the captured kinematics for test C15-I25-D10. In this test, 10 mm particles were used to impact the rigid barrier that had a basal clearance of $H_c/D = 1.5$. The channel was inclined at 25° . As the flow front arrived at the barrier (Fig. 6a), only dispersed material at the flow front passed through the basal clearance. The retained material (Fig. 6b) provided additional confining stress to resist the discharge of material through the clearance (Fig. 6c). The increasing shear resistance provided from overlying particles eventually jammed the flow and the impact process reached a static state (Fig. 6d), which is similar to that reported by Janda et al. (2008).

When $H_c/D = 1.5$, the barrier retained more than 98% of the initial flow volume. Compared with results reported by Wendeler and Volkwein (2015), the result in this study indicates that for dry monodisperse flow, a height that is 1.5 times of the particle size for the basal clearance can provide quite a high retention volume. For a barrier with a basal clearance that had a relative opening $H_c/D \geq 3$, jamming was not observed in this study. By allowing the material to freely discharge to downstream through the basal clearance, overflow volume can potentially be reduced. This implies that a basal clearance can indirectly minimise the threat posed by scouring from overflow.

Effects of basal clearance on granular jump process

Figure 7 shows a comparison of the measured jump height h_j normalised by flow depth h_i with different basal clearance heights, H_c/D , at different Froude conditions. The basal clearance height, H_c/D , and Froude number were selected as the horizontal axes of Figs. 7a and 7b, respectively, to discern the effects of these two parameters. Figure 7a shows that larger basal clearances reduced jump height for finer granular material ($D = 3$ mm, $H_c/D \geq 5.0$) by up to 34%. By contrast, for coarser granular flow ($D = 10$ mm, $H_c/D \geq 1.5$), the jump height increased less than 10% in this study compared to that of a barrier without basal clearance. An exception to this trend was observed when $Fr = 3.2$ and $H_c/D = 3.0$. Under such conditions, a 15% decrease in the jump height was observed. The decrease of jump height was because more material passed through the clearance and therefore less material was available for the granular jump. Moreover, due to the reduced lateral earth pressure at the basal clearance, the momentum of the flow would be much easier to transfer downstream instead of transferring upwards. The increase of jump height was due to the less material discharged to downstream and the intensive shearing induced during the discharge process.

More specifically, one would expect enhanced shearing between grains of the deposited material and the discharge passing through the clearance. Such shear-induced stresses between grains can be represented using the theory proposed by

Bagnold (1954). Figure 8a shows two layers of particles subjected to a shear rate $\dot{\gamma}$ in a densely packing granular flow. The upper layer represents the deposited flow and the lower layer represents the discharge flow. As the granular assembly is sheared, a velocity gradient δv develops and particles interact between the two layers. There are two types of grain interaction, one type results in dispersive stress P_y in the normal direction of the flow, while the other type results in grain shear stress P_x along the direction of flow. These stresses are given as follows:

$$(20) \quad P \sim \rho_s \dot{\gamma}^2 D^2$$

$$(21) \quad P = \frac{P_x}{\sin \alpha_c} = \frac{P_y}{\cos \alpha_c}$$

Equation (20) shows that the grain collisional stress P is proportional to grain density ρ_s , square of the shear rate $\dot{\gamma}^2$ and particle diameter square D^2 . The grain collisional stress P can be divided into grain shear stress P_x and grain dispersive stress P_y , and is expressed in eq. (21). Here, α_c is an angle, which is dependent on the direction of collision and whether the rotation of grains occurs (Bagnold 1954). Equations (20) and (21) suggest that as flow discharges through the basal clearance (Fig. 8b), collisions between the arrested material and discharging flow may increase both the grain dispersive and grain shear stresses. Larger particles and higher Fr lead to higher dispersive stresses P_y , which is reflected in the increase of jump height.

The dashed line in Fig. 7b is the estimated jump height based on eq. (1) with $k = 1$

and $\rho_i = \rho_j$. The result from Fig. 7b shows that the analytical solution of eq. (1) can overestimate the jump height when $Fr = 3.2\sim 3.4$. The jump height can be overestimated by up to twice the measured values. In addition, eq. (1) underestimates the jump height by up to 15% when $Fr = 4.5\sim 5.7$. A reason for the underestimation is that eq. (1) is meant for predicting the jump height of granular flows with an internal friction angle larger than channel inclination (Hákonardóttir et al. 2003b). When the internal friction angle is smaller than the slope angle, the elevated surface will be unstable and need to readjust to the repose angle thereby causing an increase in the jump height. Albaba et al. (2018) proposed an alternative approach to estimate the increased jump height by calculating the length of the granular jump along the flow direction. Since this method requires the input of the incoming flow velocity and flow depth, predicting the jump in a practical sense can be challenging. Notwithstanding, the 15% underestimation of the jump height in this study is not unacceptable and eq. (1) is suitable for estimating the jump height of granular flow impacting a barrier with basal clearance.

In summary, results show that a closed barrier is not the most conservative scenario for calculating the jump height. A basal clearance that has a relative opening $H_c/D \leq 3$ may induce an increase of jump height of up to 8%. A basal clearance that has relative openings of $H_c/D = 5$ and 10 may result in a reduction of jump heights by up to 11% and 34%, respectively. Even for $H_c/D = 5$, the reduction of the granular jump

was only up to 11% compared to that of a closed barrier. Therefore, a barrier with a basal clearance with an $H_c/D \geq 10$ is recommended for mitigating granular jumps.

Effects of basal clearance on impact force

Figure 9 shows the measured peak impact force exerted on barriers with different basal clearances for fine (Fig. 9a) and coarse (Fig. 9b) granular flows. The impact forces calculated from eqs. (11) and (16) are shown for reference. Furthermore, loadings under different Fr are compared. Using eq. (11) with a theoretical dynamic pressure coefficient $\alpha = 1.0$, the flow is assumed to be incompressible, and v_i and h_i were measured from the open channel tests.

Figure 9 shows that the measured peak force for fine-grained flows decreased with an increasing basal clearance height. By contrast, the measured peak force for coarse particles when $H_c/D = 1.5$ increased by up to 6% compared to a barrier without a basal clearance. The peak force decreased by 13% to 40% when $H_c/D = 3.0$. The increase of peak impact force suggests that the impact force on a barrier with smaller basal clearance, $H_c/D \leq 1.5$, cannot effectively be reduced compared with a barrier without a basal clearance. The reason that a barrier with $H_c/D = 1.5$ did not attenuate the impact force was only up to 2% of the flow volume discharged to downstream. This small discharge volume had a negligible effect on the decrease of the overall impact load.

By contrast, when $H_c/D \geq 3.0$, a more obvious reduction in the peak impact force can be found. When $H_c/D \geq 3.0$, the reduction in the peak impact force ranged from 11% to 18%, compared to barrier without basal clearances, for Fr from 5.3 to 5.7. When H_c/D ranged from 3 to 5, the reduction of peak impact force was from 20% to 29% and 35% to 40% for flows with Fr from 4.5 to 4.6, and from 3.2 to 3.4, respectively. Larger reductions in impact force, from 43% to 77%, were observed for Fr from 3.4 to 4.6 with a clearance of $H_c/D = 10.0$. Results show that Fr governed the reduction of impact force exerted on barriers with basal clearances, and the basal clearance had less effect on more inertial flows. Details of the reduction of peak force on the barrier and the jamming condition in each test are summarised in Table 1. Result in Table 1 reveals that for barrier configurations where jamming did not occur at the basal clearance, the discharge of the flow led to smaller static force on the barrier, which in turn reduced the peak impact force on the barrier.

Performance of newly proposed analytical model for barrier with basal clearance

Results show that the proposed impact model in this study can reliably predict the decreasing trend of the impact force with an increasing basal clearance height at different Froude conditions (Figs. 9a and 9b). However, the impact force was underestimated for finer granular flows ($D = 3$ mm) (Fig. 9a) with Froude numbers of 4.6 and 5.7. The lower than expected impact loads may be attributed to the smaller jump heights as shown in Fig. 7b. The finding demonstrates the importance of a reliable

momentum jump model for predicting the impact force. Figure 9b shows that the proposed model in this study overestimates the impact force exerted by coarse granular flow ($D = 10$ mm). However, the proposed model still provides a reasonable upper bound compared with the constant theoretical impact forces predicted by using eq. (11) without considering the effects of basal clearance.

Attention should also be placed on the observation that the theoretical impact force for fine granular flow with $H_c/D > 10$ and for coarse granular flow with $H_c/D > 3$ may not be valid using the proposed impact model since the barriers with a basal clearance can lose its regulatory function once the basal clearance exceeds a critical height. This critical basal height can be determined using the maximum flow depth. A comparison of results from the proposed impact model and the measured results shows reasonable agreement.

However, the proposed analytical model was only evaluated against idealized monodisperse dry granular flows in this study. For debris flow, the fluid phase plays an integral role in regulating the flow dynamics (Iverson 1997; McArdell et al. 2007). More specifically, excess pore water pressures are generated as a granular assembly is sheared. Correspondingly, contact stresses are reduced. This implies that less material is expected to be retained by barriers with basal clearances for wet flows compared to that of dry granular flows.

Scale effects are governed by the interaction between the solid and fluid phases (Iverson 2015). However, the proposed impact model in this study treats the flow as an incompressible equivalent fluid, which neglects the particle-particle and particle-fluid interactions. Correspondingly, the simple impact model can be used for any scenario by treating the flow as an equivalent fluid (Hungry 1995). Test results (Fig. 9) also show that the current model does not explicitly consider the effects of a small basal clearance which cannot have an impact force reduction compared to barrier without basal clearance when $H_c/D = 1.5$.

More importantly, findings from this study provide a basis for evaluating existing recommendations for basal clearances in literature. For example, the basal clearance heights of some proprietary steel net barriers in the field range from 0.5 m to 1.5 m based on that reported by Sze and Lam (2017). However, their report does not specify whether the recommended range of clearance is for reducing the frontal impact force, minimising the jump height, reducing the serviceability required by the barrier or maximising the volume retained. Results from this study reveal that the optimum clearance is different depending on its intended function. For example, this study recommends an optimum clearance of $H_c/h_i \geq 0.6$ for reducing the impact force and an optimum clearance of $H_c/h_i \geq 0.9$ for reducing the jump height. Although the scope of

this study was limited to idealized dry granular flows, results suggest that even for more complex flows, the basal clearance is different depending on its intended function.

Load distribution along the barrier

Figure 10 compares the load distribution along the height of barriers with different basal clearances at a channel inclination of 35° . Peak loads from the four load cells are shown. Results show increases in peak load near the base of the barrier, compared to that of a closed barrier by 13% and 27% for the fine particles ($Fr = 5.7$, $H_c/D = 10.0$) and the coarse particles ($Fr = 5.3$, $H_c/D = 3.0$), respectively. The higher peak loads were attributed to the disruption of the dead zone near the basal clearance. A dead zone can attenuate the dynamic impact of the subsequent flow on the barrier by redirecting the flow (Ng et al. 2017b).

In summary, the newly-proposed model is suitable for predicting the impact force on barriers with basal clearance. When $H_c/D \geq 3.0$, the peak force shows a consistent decrease with increasing basal clearance. The delay in the formation of the dead zone for barriers with clearances during the impact process can result in an increase of impact force near the base of the barrier. However, this local increase will not affect the total force exerted on the barrier.

Conclusions

A series of flume experiments were conducted to investigate the interaction between dry granular flows and a rigid barrier with a basal clearance. The effects of the basal clearance H_c/D on discharge, jump height and impact force were examined. Findings from this study are drawn as follows:

- a) A closed barrier is not the most conservative design scenario and the effects of a basal clearance cannot be ignored. Both the Froude numbers and normalised basal clearance H_c/D are key design considerations when assessing the discharge, jump height and impact force.
- b) Both the momentum-based jump model and a newly-proposed impact model, with consideration of a basal clearance, were evaluated. Both models reasonably predict the jump and impact force for dry granular flows with Froude condition ranging from 3.2 to 5.7.
- c) For dry monodisperse granular flows, a basal clearance of $H_c \geq 3D$ reduces the impact force by up to 77%. The jump height on the barrier can be reduced by up to 34% when $H_c = 10D$. A basal clearance height $H_c \geq 3D$ is suggested to reduce the impact force and overflow volume in multiple-barrier systems.
- d) For dry monodisperse granular flows, a basal clearance $H_c \leq 1.5D$ can achieve a retention volume by more than 98% of the total volume. However, neither the jump height nor the impact force is suppressed.

Acknowledgements

The authors are grateful for the financial sponsorship from the National Natural Science Foundation of China (51709052). The authors are also grateful for financial support from the theme-based research grant T22-603/15-N and the General Research Fund 16209717 provided by the Research Grants Council of the Government of Hong Kong Special Administrative Region, China. The authors would like to gratefully acknowledge the support of the HKUST Jockey Club Institute for Advanced Study.

References

- Albaba, A., Lambert, S., and Faug, T. 2018. Dry granular avalanche impact force on a rigid wall: Analytic shock solution versus discrete element simulations. *Physical Review E*, **97**(5), 052903. doi:10.1103/PhysRevE.97.052903.
- Armanini, A., Larcher, M., and Odorizzi, M. 2011. Dynamic impact of a debris flow front against a vertical wall. *In Proceedings of the 5th International Conference on Debris-Flow Hazards Mitigation: Mechanics, Prediction and Assessment*, Padua, Italy, pp. 1041–1049.
- Bagnold, R.A. 1954. Experiments on a gravity-free dispersion of large solid spheres in a Newtonian fluid under shear. *Proc. R. Soc. A*, **225**(1160): 49–63. doi:10.1098/rspa.1954.0186

- Caccamo, P., Faug, T., Bellot, H., and Naaim-Bouvet, F. 2011. Experiments on a dry granular avalanche impacting an obstacle: dead zone, granular jump and induced forces. *WIT Transactions on The Built Environment*, **115**: 53–62.
- Cardano, G., and Spon, C. 1968. *Ars magna (1545)*. *Opera Omnia*, **4**, 221–302.
- Chen, H., Liu, J., and Zhao, W. 2016. Effects of Y-type spillway lateral contraction ratios on debris-flow patterns and scour features downriver of a check dam. *Nat. Hazards Earth Syst. Sci.*, **16**(11): 2433–2442. doi:10.5194/nhess-16-2433-2016.
- Chiari, M., Moser, M., Trojer, M., and Hübl, J. 2016. Physical scale experiments on torrential filter structures. *In EGU General Assembly Conference Abstracts (Vol. 18, p. 6406)*, Vienna, Austria.
- Choi, C.E., Ng, C.W.W., Song, D., Kwan, J.S.H., Shiu, H.Y.K., Ho, K.K.S., and Koo, R.C.H. 2014. Flume investigation of landslide debris-resisting baffles. *Can. Geotech. J.*, **51**(5): 540–553. doi:10.1139/cgj-2013-0115.
- Choi, C.E., Au-Yeung, S., Ng, C.W.W., and Song, D. 2015. Flume investigation of landslide granular debris and water runup mechanisms. *Géotechnique Letters*, **5**(1): 28–32. doi:10.1680/geolett.14.00080.
- Comiti, F., Lenzi, M., and Mao, L. 2013. Local scouring at check-dams in mountain rivers. *In Check dams, morphological adjustments and erosion control in torrential streams*. Edited by C. Conesa-Garcia and M.A. Lenzi. Nova Science Publisher, Hauppauge, New York, pp. 263–282.
- Faug, T., Lachamp, P., and Naaim, M. 2002. Experimental investigation on steady

granular flows interacting with an obstacle down an inclined channel: study of the dead-zone upstream from the obstacle. Application to interaction between dense snow avalanches and defence structures. *Nat. Hazards Earth Syst. Sci.*, **2**(3/4): 187–191. doi:10.5194/nhess-2-187-2002.

Faug, T., Caccamo, P., and Chanut, B. 2012. A scaling law for impact force of a granular avalanche flowing past a wall, *Geophys. Res. Lett.*, **39**, L23401, doi:10.1029/2012GL054112.

Faug, T. 2015a. Depth-averaged analytic solutions for free-surface granular flows impacting rigid walls down inclines. *Physical Review E*, **92**, 062310. doi:10.1103/PhysRevE.92.062310.

Faug, T. 2015b. Macroscopic force experienced by extended objects in granular flows over a very broad Froude-number range. *Eur. Phys. J. E*, **38**: 34. doi:10.1140/epje/i2015-15034-3.

Faug, T., Childs, P., Wyburn, E., and Einav, I. 2015. Standing jumps in shallow granular flows down smooth inclines. *Physics of Fluids*, **27**, 073304. doi:10.1063/1.4927447.

Gems, B., Wörndl, M., Gabl, R., Weber, C., and Aufleger, M. 2014. Experimental and numerical study on the design of a deposition basin outlet structure at a mountain debris cone, *Nat. Hazards Earth Syst. Sci.*, **14**, 175–187, doi:10.5194/nhess-14-175-2014.

Glasse, T. 2013. Hydrology and check dams analysis in the debris flow context of Illgraben torrent. MAS practical research project, Swiss Federal Institute of

- Technology, Zurich, Switzerland.
- Gray, J.M.N.T., Tai, Y.C., and Noelle, S. 2003. Shock waves, dead zones and particle-free regions in rapid granular free-surface flows. *J. Fluid Mech.* **491**: 161–181. doi:10.1017/S0022112003005317.
- Hákonardóttir, K.M., Hogg, A.J., Batey, J., and Wood, A.W. 2003a. Flying avalanches. *Geophys. Res. Lett.*, **30**(23): 1–4. doi:10.1029/2003GL018172
- Hákonardóttir, K. M., Hogg, A. J., and Jóhannesson, T. 2003b. A laboratory study of the interaction between supercritical, shallow flows and dams. Icelandic Meteorological Office (Vedurstofa Islands) Report 03038.
- Hübl, J., Strauss, A., Holub, M., and Suda, J. 2005. Structural mitigation measures. *In* 3rd Probabilistic Workshop: Technical Systems + Natural Hazards, Vienna, Austria, pp. 115–126.
- Hübl, J., Suda, J., Proske, D., Kaitna, R., and Scheidl, C. 2009. Debris flow impact estimation. *In* Proceedings of the 11th International Symposium on Water Management and Hydraulic Engineering, Ohrid, Macedonia, pp. 1–5.
- Hungr, O. 1995. A model for the runout analysis of rapid flow slides, debris flows, and avalanches. *Canadian Geotechnical Journal*, **32**(4), 610-623. doi:10.1139/t95-063.
- Iverson, R.M. 1997. The physics of debris flows. *Reviews of geophysics*, **35**(3), 245–296. doi:10.1029/97RG00426.
- Iverson, R.M. 2015. Scaling and design of landslide and debris-flow experiments. *Geomorphology*, **244**, 9–20. doi:10.1016/j.geomorph.2015.02.033.

- Iverson, R.M., George, D. L., and Logan, M. 2016. Debris flow runup on vertical barriers and adverse slopes. *J. Geophys. Res.: Earth Surf.*, **121**: 2333–2357. doi:10.1002/2016JF003933.
- Janda, A., Zuriguel, I., Garcimartín, A., Pagnaloni, L. A., and Maza, D. 2008. Jamming and critical outlet size in the discharge of a two-dimensional silo. *EPL (Europhysics Letters)*, **84**(4), 44002. doi:10.1209/0295-5075/84/44002.
- Jóhannesson, T., Gauer, P., Issler, D., and Lied, K. 2009. The design of avalanche protection dams: recent practical and theoretical developments. European Commission, Belgium.
- Ketterhagen, W. R., Curtis, J. S., Wassgren, C. R., and Hancock, B. C. 2009. Predicting the flow mode from hoppers using the discrete element method. *Powder technology*, **195**(1): 1–10. doi:10.1016/j.powtec.2009.05.002.
- Kwan, J.S.H. 2012. Supplementary technical guidance on design of rigid debris resisting barriers. Technical Note No. TN 2/2012. Geotechnical Engineering Office, Civil Engineering and Development Department, The HKSAR Government.
- Kwan, J. S. H., Koo, R. C. H., and Ng, C. W. W. 2015. Landslide mobility analysis for design of multiple debris-resisting barriers. *Canadian Geotechnical Journal*, **52**(9): 1345–1359. doi:10.1139/cgj-2014-0152.
- MLR. 2006. Specification of Geological Investigation for Debris Flow Stabilization. DZ/T 0220-2006. National Land Resources Department, China. [In Chinese.]
- Moase, E., Strouth, A., Jakob, M., and Stead, D. 2017. Guidance for steep creek

hazard mitigation design in Canada. *In* Proceedings of GeoOttawa, 70th Canadian Geotechnical Conference and 12th joint CGS/IAH-CNC Groundwater Conference, Ottawa, Canada, 1 to 4 Oct. 2017.

McArdell, B.W., Bartelt, P., and Kowalski, J. 2007. Field observations of basal forces and fluid pore pressure in a debris flow. *Geophysical Research Letters*, **34**(7). doi:10.1029/2006GL029183.

Naaïm - Bouvet, F., Faug, T., and Naaïm, M. 2004. Dense and powder avalanches: momentum reduction generated by a dam. *Ann. Glaciol.*, **38**, 373–378. doi:10.3189/172756404781815185.

Nagl, G., Hübl, J., and Chiari, M. Ein Vergleich Von Dynamischen Einwirkungen Von Muren An Einem Starren Bauwerk Und Einer Flexiblen Netzsperrre In Einem Kleinmaßstäblichen Modellversuch. 2016a. *In* Proceedings of GeoTirol 2016 Annual Meeting DGGV, Innsbruck, Austria. [In German.]

Nagl, G., Hübl, J., and Chiari, M. 2016b. Experimental testing of impact force on rigid and flexible barriers - A comparison. *In* EGU General Assembly Conference Abstracts (Vol. 18, p. 6991), Vienna, Austria.

Ng, C.W.W., Choi, C.E., Liu, L.H.D., Wang, Y., Song, D., and Yang, N. 2017a. Influence of particle size on the mechanism of dry granular run-up on a rigid barrier. *Géotechnique Letters*, **7**(1): 79–89. doi:10.1680/jgele.16.00159.

Ng, C.W.W., Song, D., Choi, C.E., Kwan, J.S.H., Koo, R.C.H., and Pun, W.K. 2017b.

Impact mechanisms of granular and viscous flows on rigid and flexible barriers.

Canadian Geotechnical Journal, **54**(2): 188–206. doi:10.1139/cgj-2016-0128.

Ng, C.W.W., Choi, C.E., Koo, R.C.H., Goodwin, G.R., Song, D., and Kwan, J.S.H. 2018.

Dry granular flow interaction with dual-barrier systems. *Géotechnique*, **68**(5): 386–399. doi: 10.1680/jgeot.16.P.273.

NILIM. 2007. Manual of technical standard for establishing sabo master plan for debris flow and driftwood. Technical Note of NILIM No. 364. Natural Institute for Land and Infrastructure Management, Ministry of Land, Infrastructure and Transport, Japan. [In Japanese.]

Piton, G., and Recking, A. 2015. Design of sediment traps with open check dams. I: Hydraulic and deposition processes. *Journal of Hydraulic Engineering*, **142**(2), 04015045. doi:10.1061/(ASCE)HY.1943-7900.0001048.

Scheidl, C., Chiari, M., Müllegger, M., and Proske, D. 2012. Estimation of debris-flow impact forces using a small scale modelling approach. *In* 12th Congress Interpraevent, Grenoble, France.

Scheidl, C., Chiari, M., Kaitna, R., Müllegger, M., Krawtschuk, A., Zimmermann, T., and Proske, D. 2013. Analysing debris-flow impact models, based on a small scale modelling approach. *Surveys in Geophysics*, **34**(1), 121–140. doi:10.1007/s10712-012-9199-6.

Sovilla, B., Faug, T., Köhler, A., Baroudi, D., Fischer, J.T., and Thibert, E. 2016.

Gravitational wet avalanche pressure on pylon-like structures. *Cold Regions Sci. Technol.* **126**(2016): 66–75, doi:10.1016/j.coldregions.2016.03.002.

Speerli, J., Hersperger, R., Wendeler, C., and Roth, A. 2010. Physical modeling of debris flows over flexible ring net barriers. *In* Proceedings of the Seventh International Conference on Physical Modelling in Geotechnics (ICPMG), Zurich, Switzerland. Edited by S. Springman, J. Laue, and L. Seward. Taylor & Francis Group. pp. 1285–1290.

Sun, H.W., and Law, R.P.H. 2015. A preliminary study on impact of landslide debris on flexible barriers. GEO Report No. 309. Geotechnical Engineering Office, Civil Engineering and Development Department, The HKSAR Government.

Sze, E., and Lam, H. 2017. Some suggested detailing of flexible barriers traversing a stream course for drainage purposes. Technical Note No. TN 3/2017. Geotechnical Engineering Office, Civil Engineering and Development Department, The HKSAR Government.

Tordesillas, A., Steer, C.A.H., and Walker, D.M. 2014. Force chain and contact cycle evolution in a dense granular material under shallow penetration. *Nonlinear Processes in Geophysics*, **21**(2): 505–519. doi:10.5194/npg-21-505-2014.

VanDine, D.F. 1996. Debris Flow Control Structures for Forest Engineering. Ministry of Forests, British Columbia, Canada, 68 p.

Volkwein, A. 2014. Flexible debris flow barriers: Design and application. WSL Berichte,

18. Birmensdorf, Swiss Federal Institute for Forest, Snow and Landscape Research WSL. 29 p.

Wendeler, C., Volkwein, A., Roth, A., Herzog, B., Hahlen, N., and Wenger, M. 2008. Hazard prevention using flexible multi-level debris flow barrier. In *Interpraevent* (Vol. 1, pp. 547–554).

Wendeler, C, and Volkwein, A. 2015. Laboratory tests for the optimization of mesh size for flexible debris-flow barriers. *Nat. Hazards Earth Syst. Sci.*, **15**: 2597–2604. doi:10.5194/nhess-15-2597-2015.

Wendeler, C., Volkwein, A., McArdell, B. W., and Bartelt, P. 2018. Load model for designing flexible steel barriers for debris flow mitigation. *Canadian Geotechnical Journal*, doi:10.1139/cgj-2016-0157.

Wieser, N. 2014. Physikalische Modellierung zur Optimierung von flexiblen Murbarrieren am Beispiel Trattenbach. Master Thesis, Institut für Alpine Naturgefahren (IAN), BOKU-Universität für Bodenkultur, pp 110. [In Deutsch.]

White, D.J., Take, W.A., and Bolton, M.D. 2003. Soil deformation measurement using particle image velocimetry (PIV) and photogrammetry. *Géotechnique*, **53**(7): 619–631. doi:10.1680/geot.2003.53.7.619.

WSL. 2008. Integral risk management of extremely rapid mass movements. Swiss Federal Institute for Snow and Avalanche Research. Available from <http://irasmos.slf.ch/> [accessed 5 September 2018].

Zanuttigh, B., and Lamberti, A. 2006. Experimental analysis of the impact of dry

avalanches on structures and implication for debris flow. *Journal of Hydraulic Research*, **44**(4): 522–534. doi:10.1080/00221686.2009.9522009.

List of Table

Table 1. Summary of test programme and results.

List of Figures

Fig. 1. Schematic of basal clearance in rigid and flexible barriers: (a) rigid slot dam; (b) flexible steel net barrier.

Fig. 2. Side schematic of flow impacts on a barrier with basal clearance.

Fig. 3. Side schematic of the test set-up (a) and the instrumented barrier (b).

Fig. 4. Side schematic of the control test at different time to determine the flow velocity: (a) t_1 , when the flow is 50 mm upstream the barrier location; (b) t_2 , when the flow is 50 mm downstream the barrier location.

Fig. 5. Observed flow kinematics (left) and PIV analysis (right) of test C30-I35-D10 at different time: (a) $t = 0.15$ s; (b) $t = 0.40$ s; (c) $t = 1.20$ s.

Fig. 6. Observed discharge and jamming of test C15-I25-D10: (a) $t = 0.00$ s; (b) $t = 0.10$ s; (c) $t = 0.40$ s; (d) $t = 1.30$ s.

Fig. 7. Comparison of measured peak jump height at different Froude conditions with (a) different basal clearance heights and (b) the momentum jump model ($k = 1$ and $\rho_i = \rho_j$).

Fig. 8. Side schematic of grain stresses during discharging process: (a) densely packing resisted flow layer (upper) and discharging flow layer (lower) moving at a certain shear rate; (b) intensive collisions induced by basal clearance discharge.

Fig. 9. Comparison of measured peak impact load at different basal clearance heights

and Froude conditions: (a) flow with particle diameter 3mm; (b) flow with particle diameter 10mm.

Fig. 10. Measured distributed impact force along the barrier for different basal clearance heights: (a) flow with particle diameter 3mm at $Fr = 5.7$; (b) flow with particle diameter 10mm at $Fr = 5.3$.

Table 1. Summary of test programme and results

Test ID	Basal clearance, H_c (mm)	Flume inclination ($^{\circ}$)	Particle diameter, D (mm)	H_c/D	Flow kinematics			Impact force results		Jamming at the basal clearance
					Frontal velocity, v (m/s)	Flow depth*, h (mm)	Froude number, Fr	Peak total force (N)	Reduction proportion of peak total force (%)	
I15-D3	—	15	3	—	1.5	21	3.4	—	—	—
I25-D3		25			2.2	26	4.6			
I35-D3		35			3.0	35	5.7			
I15-D10		15	10		1.8	31	3.2			
I25-D10		25			2.6	37	4.5			
I35-D10		35			3.2	46	5.3			
C0-I15-D3	0	15	3	0.0	1.5	21	3.4	11.3	0	
C0-I25-D3		25			2.2	26	4.6	61.1		
C0-I35-D3		35			3.0	35	5.7	121.3		
C0-I15-D10		15	10		1.8	31	3.2	21.1		
C0-I25-D10		25			2.6	37	4.5	80.1		
C0-I35-D10		35			3.2	46	5.3	152.3		
C15-I15-D3	15	15	3	5.0	1.5	21	3.4	7.4	35	No
C15-I25-D3		25			2.2	26	4.6	43.5	29	
C15-I35-D3		35			3.0	35	5.7	108.4	11	
C15-I15-D10		15	10	1.5	1.8	31	3.2	23.5	-11	Yes
C15-I25-D10		25			2.6	37	4.5	83.8	-5	
C15-I35-D10		35			3.2	46	5.3	154.3	-1	
C30-I15-D3	30	15	3	10.0	1.5	21	3.4	2.6	77	No
C30-I25-D3		25			2.2	26	4.6	34.8	43	
C30-I35-D3		35			3.0	35	5.7	99.7	18	
C30-I15-D10		15	10	3.0	1.8	31	3.2	12.7	40	
C30-I25-D10		25			2.6	37	4.5	63.8	20	
C30-I35-D10		35			3.2	46	5.3	132.5	13	

* The flow depth is the maximum flow depth at the barrier location from control tests.

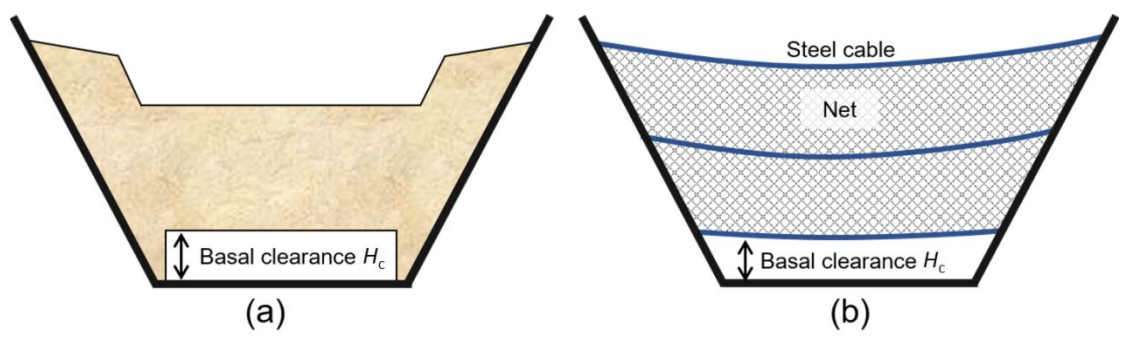


Fig. 1. Schematic of basal clearance in rigid and flexible barriers: (a) rigid slot dam; (b) flexible steel net barrier.

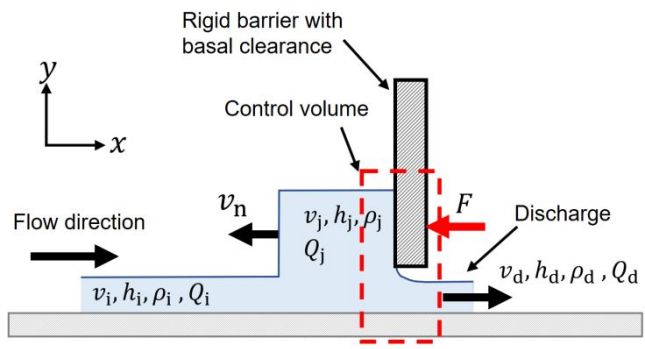


Fig. 2. Side schematic of flow impacts on a barrier with basal clearance.

Can. Geotech. J. Downloaded from www.nrcresearchpress.com by UNIV LIBRARY OF HONG KONG UNIV OF on 06/25/19
For personal use only. This Just-IN manuscript is the accepted manuscript prior to copy editing and page composition. It may differ from the final official version of record.

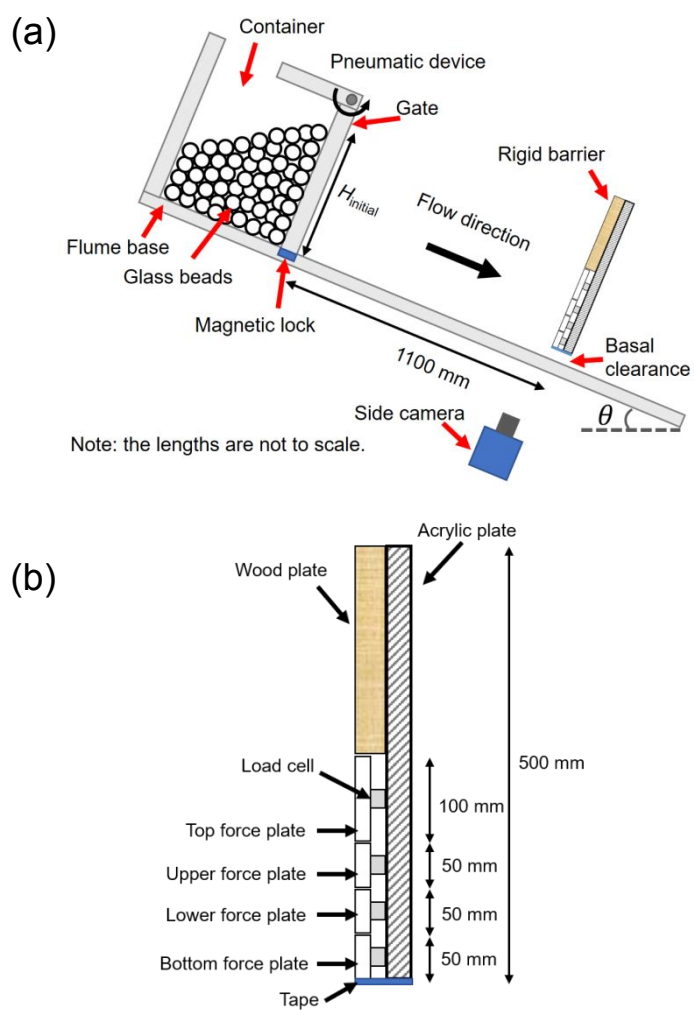


Fig. 3. Side schematic of the test set-up (a) and the instrumented barrier (b).

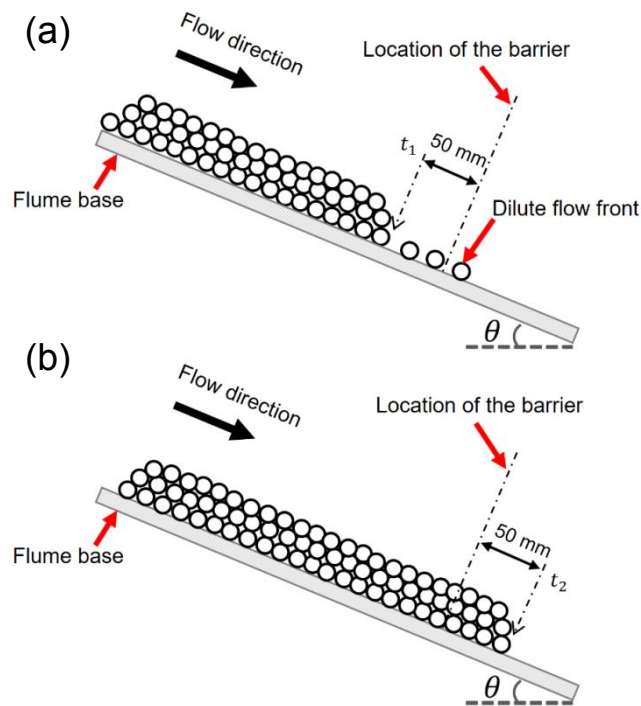


Fig. 4. Side schematic of the control test at different time to determine the flow velocity: (a) t_1 , when the flow is 50 mm upstream the barrier location; (b) t_2 , when the flow is 50 mm downstream the barrier location.

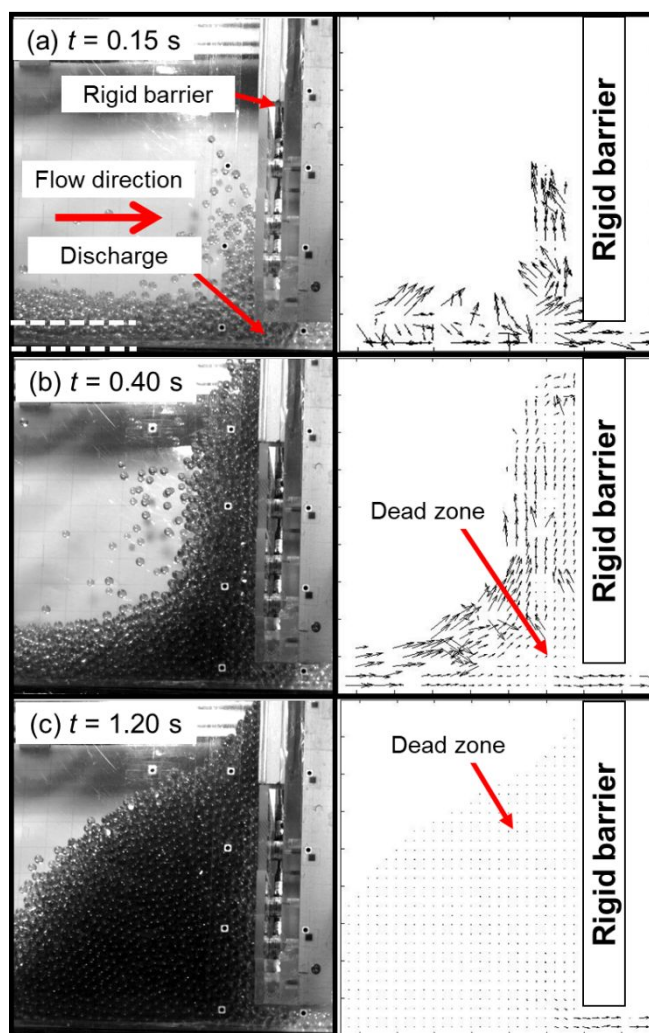


Fig. 5. Observed flow kinematics (left) and PIV analysis (right) of test C30-I35-D10 at different time: (a) $t = 0.15$ s; (b) $t = 0.40$ s; (c) $t = 1.20$ s.

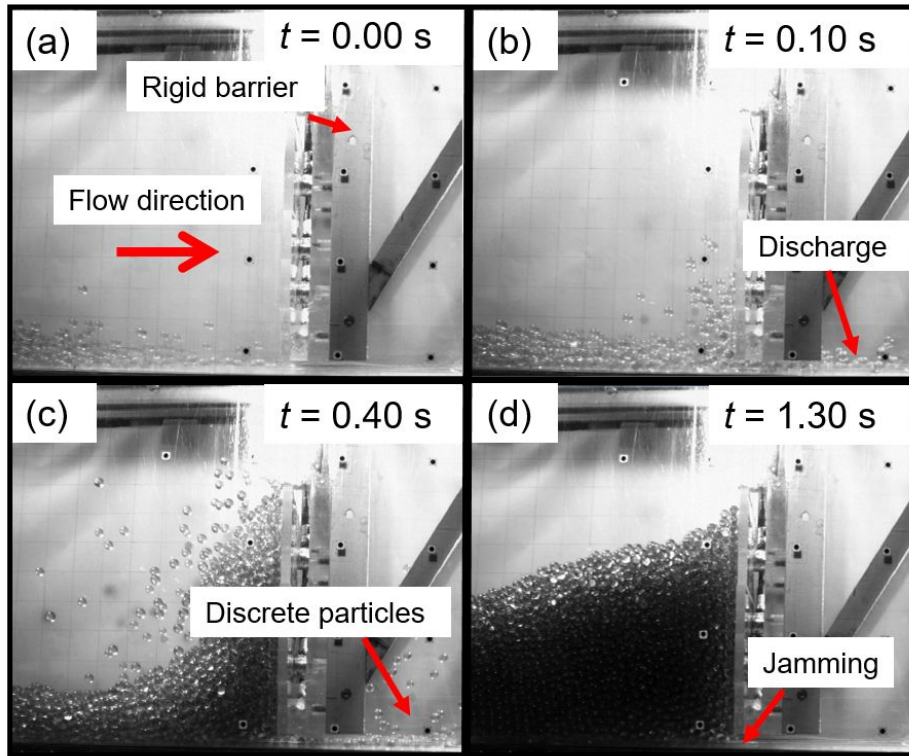


Fig. 6. Observed discharge and jamming of test C15-I25-D10: (a) $t = 0.00$ s; (b) $t = 0.10$ s; (c) $t = 0.40$ s; (d) $t = 1.30$ s.

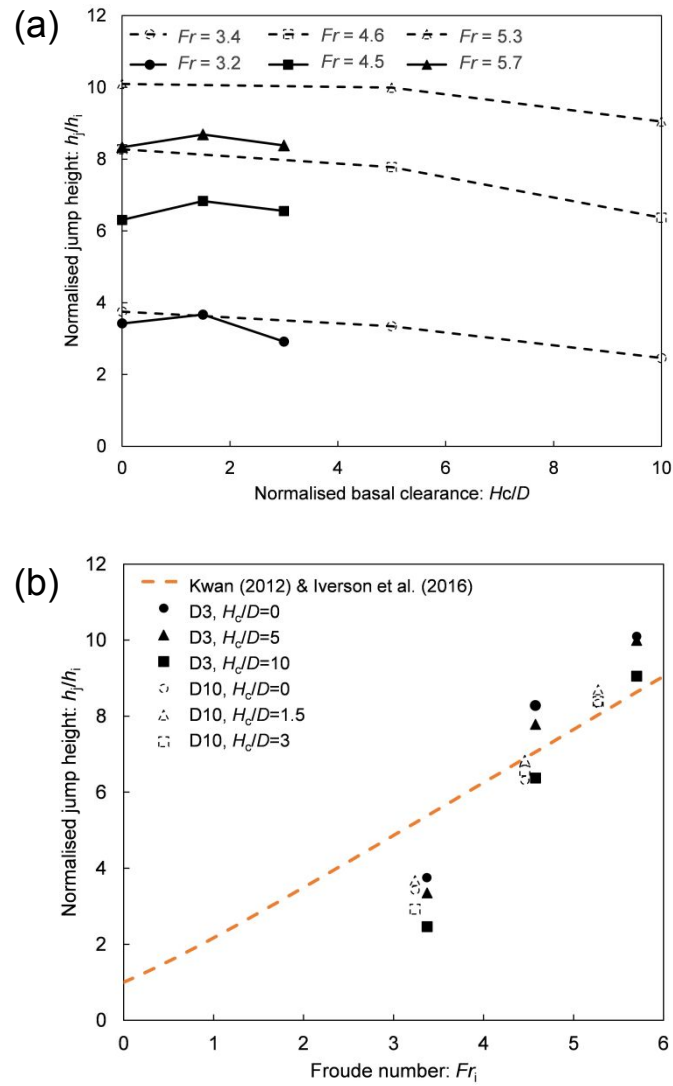


Fig. 7. Comparison of measured peak jump height at different Froude conditions with (a) different basal clearance heights and (b) the momentum jump model ($k = 1$ and $\rho_i = \rho_j$).

Can. Geotech. J. Downloaded from www.nrcresearchpress.com by UNIV LIBRARY OF HONG KONG UNIV OF on 06/25/19
For personal use only. This Just-IN manuscript is the accepted manuscript prior to copy editing and page composition. It may differ from the final official version of record.

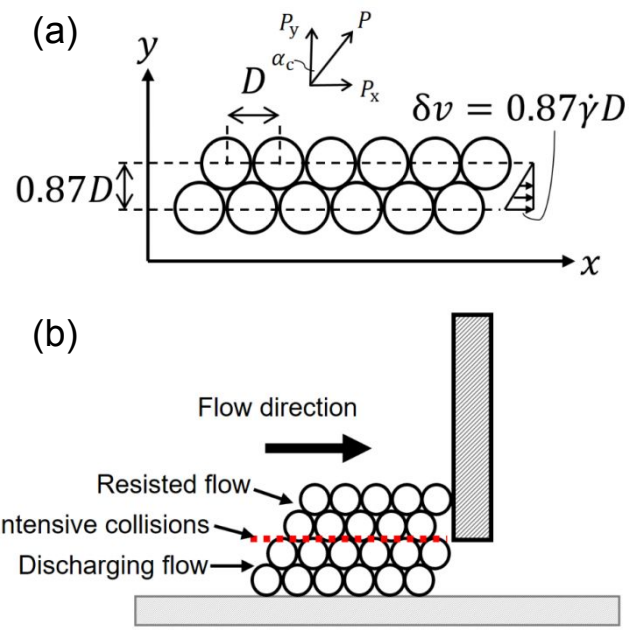


Fig. 8. Side schematic of grain stresses during discharging process: (a) densely packing resisted flow layer (upper) and discharging flow layer (lower) moving at a certain shear rate; (b) intensive collisions induced by basal clearance discharge.

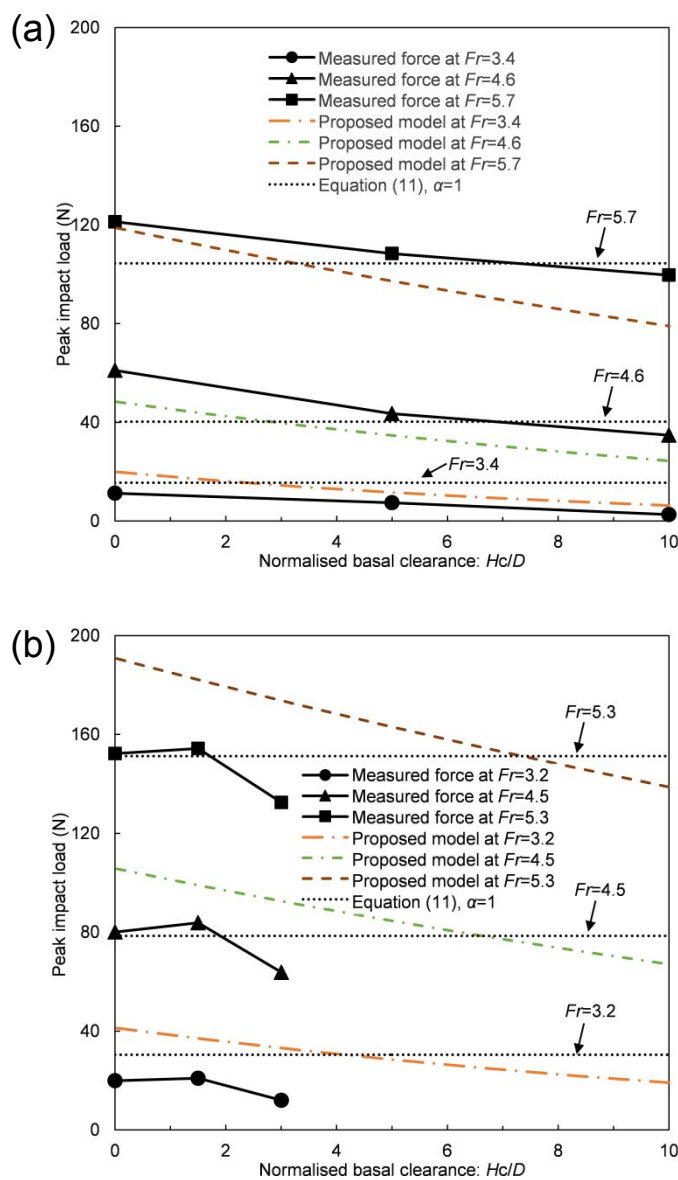


Fig. 9. Comparison of measured peak impact load at different basal clearance heights and Froude conditions: (a) flow with particle diameter 3 mm; (b) flow with particle diameter 10 mm.

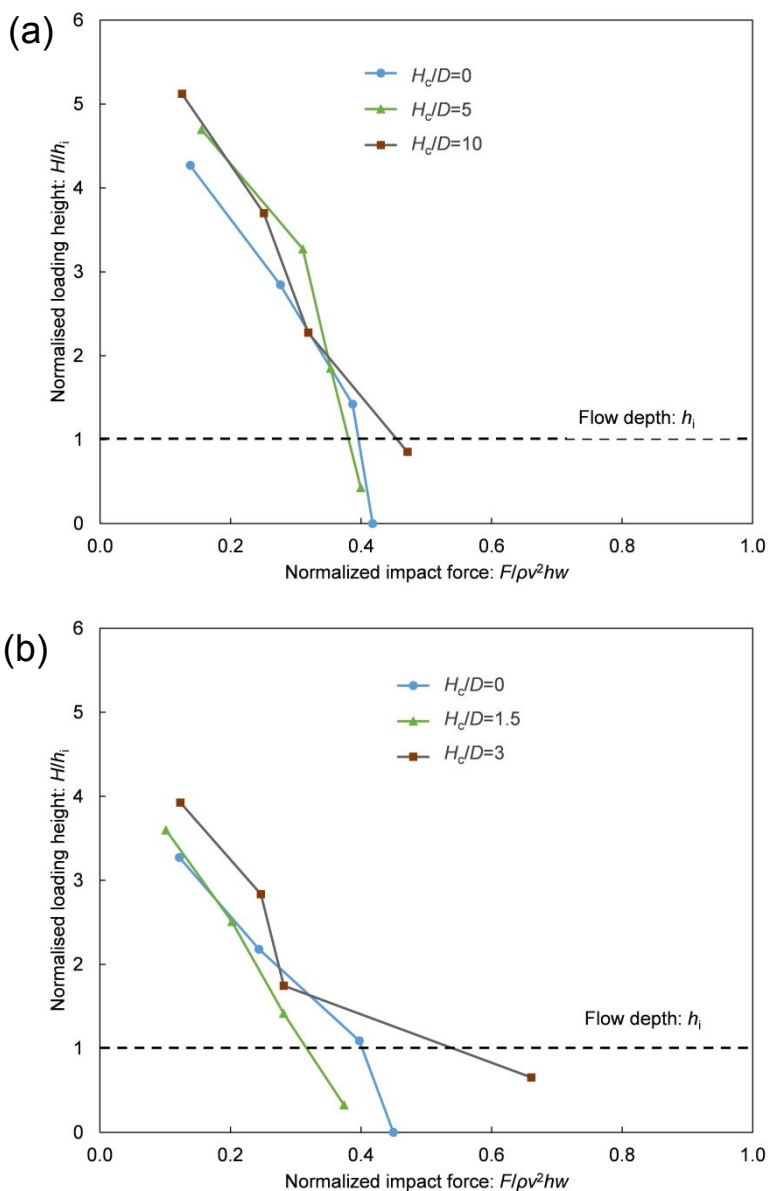


Fig. 10. Measured distributed impact force along the barrier for different basal clearance heights: (a) flow with particle diameter 3 mm at $Fr = 5.7$; (b) flow with particle diameter 10 mm at $Fr = 5.3$.